Effect of cation-vacancy superstructure on the phonon dynamics in KNi_2Se_2

Urszula D. Wdowik [●],[1] Grzegorz Jagło [●],[1] and Dominik Legut [●][2]

[1]*Institute of Technology, Pedagogical University, Podchorazych 2, 30-084 Krakow, Poland*
[2]*IT4Innovations, VSB - Technical University of Ostrava, 17. listopadu 2172/15, CZ 708 00 Ostrava-Poruba, Czech Republic*

Density functional theory investigations of effects arising from ordered structure of cation vacancies in KNi_2Se_2 are reported. The simulated cation-deficient $K_xNi_{2-y}Se_2$ phases with $x = 0.8$, $y = 0.0$, and $y = 0.4$ lie within the stoichiometry range of experimental samples produced by the self-flux method or oxidative deintercalation of a vacancy-free system. Results of the present studies indicate pronounced impact of cation vacancy superstructure on the structural, electronic, and vibrational properties of KNi_2Se_2. Revealed modifications of the local structure, atomic bond lengths, electronic, and phonon bands, which are especially noticeable in the system with both potassium and nickel deficiencies, are reflected in the simulated neutron pair-distribution functions, the phonon and Raman spectra, which are provided to facilitate both experimental verification of the predicted effects and analysis of the phase composition of a multiphase K-Ni-Se material.

I. INTRODUCTION

The ternary transition-metal dichalcogenides with general formula AT_2X_2 (A = alkali metal or Tl; T = Fe, Co, Ni; X =S, Se) are members of a large family of layered-structure compounds, adopting tetragonal quasi-two-dimensional $ThCr_2Si_2$-type structure which is formed by stacking covalently bonded transition metal-metalloid T_2X_2 layers comprised of edge-sharing TX_4 tetrahedra, with ionic A atoms. For the last few years, the layered quasi-2D AT_2X_2 systems have been the subject of numerous experimental and theoretical investigations due to their fascinating physical properties, including superconductivity in Fe-based compounds [1–3], a rich diversity of magnetic orderings in Co-based systems [4–9], and a heavy-fermion behavior at low temperatures in the Ni-based counterparts [10–13]. In most cases the composition of AT_2X_2 compounds deviates from the ideal 122 stoichiometry because of vacancies which appear in their crystal lattices. Vacancies usually occupy A- or T-cation sites, leaving the anion sublattice unaffected. The well-known example is the K-Fe-Se system, in which at least four distinct types of phases could be recognized [14]: (i) K-deficient metallic superconducting phase $K_xFe_2Se_2$ ($0.38 < x < 0.58$), (ii) Fe-deficient phase $KFe_{2-y}Se_2$ with $y = 0.4$ ($KFe_{1.6}Se_2$), and (iii) $K_xFe_{2-y}Se_2$ phase with $x = 0.8$ and $y = 0.4$. Iron vacancies in the K-Fe-Se system were observed [15–19] to form ordered structure at certain y. A regular distribution of Fe vacancies in $K_{0.8}Fe_{1.6}Se_2$ phase, which is equivalent to $K_2Fe_4Se_5$ (the so-called 245 phase), gives rise to a $\sqrt{5} \times \sqrt{5} \times 1$ superstructure [16,20]. The presence of cation vacancies in $ThCr_2Si_2$ structure results in symmetry lowering from the space group $I4/mmm$ (No. 139) to $I4/m$ (No. 87). The structurally related Ni-based compounds can also exhibit cation deficiency in the K sublattice or both K and Ni sublattices when experimental samples are prepared by the self-flux method [12,21]. Besides, the K-Ni-Se phases with variable and controllable amount of cation vacancies can be produced by the oxidative deintercalation of pristine KNi_2Se_2. It was shown [22] that $K_xNi_2Se_2$ and $K_xNi_{2-y}Se_2$ are formed at low and high oxidation levels, respectively.

Theoretical description of electronic properties of cation-deficient Ni-based 122 phases has been undertaken recently [23] within the framework of the full-potential linearized augmented plane-wave + local orbitals ($FP - LAPW + lo$) method. These simulations took into account K and Ni vacancy order in $K_{0.8}Ni_2Se_2$ and $K_{0.8}Ni_{1.6}Se_2$ compositions. They revealed significant influence of these defects on both electronic structure and Fermi surface topology of KNi_2Se_2. Following this research, we have performed density functional theory studies for the off-stoichiometric $K_xNi_2Se_2$ ($x = 0.8$) and $K_xNi_{2-y}Se_2$ ($x = 0.8$, $y = 0.4$) phases to explore the effect of vacancy superstructure on their electronic and dynamical properties. Results obtained for the K-Ni-Se systems with point defects are discussed with respect to those for pristine material as well as available experimental data reported for the nonstoichiometric K-Ni-Se compositions.

II. METHODOLOGY

A. Structural models

The simulated $K_{0.8}Ni_2Se_2$ and $K_{0.8}Ni_{1.6}Se_2$ compositions were obtained by removing the K and Ni atoms from the vacancy-free KNi_2Se_2 in a manner described in Refs. [14,23], and hence they show similar ordering pattern of cation vacancies to that encountered in the $K_xFe_{2-y}Se_2$ analogues. Ordered vacancies lower symmetry of the parent KNi_2Se_2 structure from $I4/mmm$ (No. 139) to $I4/m$ (No. 87) space group. The $K_4Ni_{10}Se_{10}$ and $K_4Ni_8Se_{10}$ model structures correspond, respectively, to $K_{0.8}Ni_2Se_2$ and $K_{0.8}Ni_{1.6}Se_2$ compositions. Created structures are shown in Fig. 1. Their unit cells are built up of interspersed Ni-Se slabs and nets of K atoms, stacked along the z axis. In the ideal KNi_2Se_2 structure of $I4/mmm$ space group, the K atoms occupy $2a(0, 0, 0)$ positions, Ni

KNi$_2$Se$_2$ **K$_x$Ni$_2$Se$_2$**   **K$_x$Ni$_{2-y}$Se$_2$**
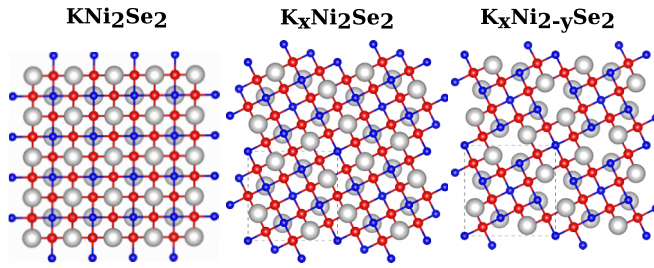
FIG. 1. The (001) projections of the $2 \times 2 \times 1$ supercells of vacancy-free KNi$_2$Se$_2$ and vacancy-containing K$_4$Ni$_{10}$Se$_{10}$ and K$_4$Ni$_8$Se$_{10}$ model structures corresponding to K$_x$Ni$_{2-y}$Se$_2$ phases with $x = 0.8$ and $y = 0.4$. Gray, red, and blue balls represent K, Ni, and Se atoms, respectively.

atoms are located at $4d(0, \frac{1}{2}, \frac{1}{4})$ positions, and Se atoms reside at $4e(0, 0, z)$ sites. The nonequivalent atomic positions for the $I4/m$ structure of K$_{0.8}$Ni$_2$Se$_2$ phase are as follows: K($8h$), Ni$_1$($4d$), Ni$_2$($16i$), Se$_1$($4e$), and Se$_2$($16i$). In the K$_{0.8}$Ni$_{1.6}$Se$_2$ phase the K, Se$_1$, and Se$_2$ atoms are found at the same Wyckoff positions as in the K$_{0.8}$Ni$_2$Se$_2$ phase, but only one nonequivalent Ni atom at ($16i$) site is present.

Despite the modeled stoichiometries of vacancy-containing K-Ni-Se systems correlate well with stoichiometries of the experimental K$_x$Ni$_2$Se$_2$ $(0.8 \leqslant x \leqslant 0.95)$ and K$_x$Ni$_{2-y}$Se$_2$ $(x = 0.63, 0.75, y = 0.25, 0.5)$ polycrystalline samples prepared by the oxidative deintercalation reaction [22] as well as K$_x$Ni$_{2-y}$Se$_2$ $(x = 0.95, y = 0.14)$ single crystals produced by the self-flux method [12,21], the simulated compositions with vacancy superstructures may not represent exactly the synthesized nonstoichiometric compounds, since the cation vacancies in realistic samples may be disordered. Most likely it was the case for recently synthesized K$_x$Ni$_2$Se$_2$ and K$_x$Ni$_{2-y}$Se$_2$ phases [12,22] as their structural parameters could be determined from the Rietveld analysis of the x-ray diffraction within the $I4/mmm$ symmetry of the KNi$_2$Se$_2$ parent phase. Otherwise, symmetries of the K-Ni-Se systems with vacancy ordered states would be lower, i.e., $I4/m$ for composition with $x = 0.8$ and $y = 1.6$.

B. Computational details

Electronic structures and the Hellmann-Feynman (HF) forces acting on atoms in the considered K-Ni-Se compositions were obtained from the density functional theory using the Vienna *ab initio* simulation package (VASP) [24], employing periodic boundary conditions, a plane wave basis set, the Perdew-Burke-Ernzerhof (PBE) generalized gradient approximation (GGA) exchange-correlation functional [25] and the projector-augmented wave (PAW) method [26] for description of the electron-ion interactions. The PAW pseudopotentials with valence electron configurations K($3p^64s^1$), Ni($3d^84s^2$), and Se($4s^24p^4$) were taken from VASP database. Calculations were performed with the energy cutoff for the plane wave expansion of 351 eV and the Monkhorst-Pack k-point mesh of $8 \times 8 \times 6$. The K$_{0.8}$Ni$_2$Se$_2$ and K$_{0.8}$Ni$_{1.6}$Se$_2$ structures were fully optimized at the convergence criteria for the total energy and the HF forces of 10^{-7} eV and 10^{-5} eV/Å, respectively. Phonons were determined within the harmonic

approximation [27] for $2 \times 2 \times 1$ supercells consisting of 192 (K$_{0.8}$Ni$_2$Se$_2$) and 176 (K$_{0.8}$Ni$_{1.6}$Se$_2$) atoms. The amplitude of atomic displacement to generate nonvanishing HF forces of ± 0.02 Å was applied. Peak intensities of the nonresonant Raman spectra (in the Stokes process) were calculated according to the expression [28]: $I \propto |\mathbf{e}_i \, \mathbf{R} \, \mathbf{e}_s|^2 \omega^{-1}(n+1)$, where $(n + 1)$ is the population factor for Stokes scattering with $n = [\exp(\hbar\omega/k_BT) - 1]^{-1}$ denoting the Bose-Einstein thermal factor, $\mathbf{e}_i$ ($\mathbf{e}_s$) is the polarization of incident (scattered) radiation, $\mathbf{R}$ is the Raman susceptibility tensor. The components of $\mathbf{R}$ tensor were determined [27,29] from derivatives of the electric polarizability tensor over the atomic displacements. Electric polarizabilities were calculated with the linear-response method implemented [30] in the VASP code. The pair-distribution functions were obtained using the PDFGUI program [31]. To compare theoretical density of phonon states to that determined from the experimental inelastic neutron scattering (INS) spectrum, the neutron-weighted phonon density of states has been evaluated as [32] $G(\omega) = \sum_i c_i \frac{\sigma_i}{M_i} f_i(\omega)$ with c_i, σ_i, and $f_i(\omega)$ denoting concentration, total neutron scattering cross section, and the partial phonon density of states for the ith atomic species, respectively. The total neutron scattering cross sections for K, Ni, and Se amount, respectively, to 1.96, 18.5, and 8.30 barn [33]. Thus, the scattering efficiencies of K, Ni, and Se equal to 0.05, 0.315, and 0.105 barn/a.m.u., respectively.

III. RESULTS AND DISCUSSION

A. Structural properties

Results of our spin-polarized calculations performed at magnetic configurations similar to those observed for K$_x$Fe$_{2-y}$Se$_2$ analogues [34] show that neither Ni nor K vacancies alter the magnetic response of the considered K-Ni-Se phases, i.e., their magnetic properties remain consistent with the Pauli paramagnetic behavior [12,13,22]. The optimized lattice constants and internal atomic coordinates of the equilibrium KNi$_2$Se$_2$, K$_{0.8}$Ni$_2$Se$_2$, and K$_{0.8}$Ni$_{1.6}$Se$_2$ compositions are summarized in Table I.

Although the K-Ni-Se phases with various stoichiometries have been identified by the x-ray diffraction experiments [12,22], their structures were refined by the Rietveld analysis under the symmetry constraints of the ideal $I4/mmm$ space group. Therefore, a direct comparison of our simulated structures containing defects with the experimental ones could not be done. Nevertheless, some general trends which follow from experiments can be outlined. In the K$_x$Ni$_2$Se$_2$ phases with $x > 0.75$ the separation between Ni-Se layers expands, whereas the Ni-Ni distances contract. These observations are reflected by the calculated K$_{0.8}$Ni$_2$Se$_2$ structure. On the other hand, the separation between Ni-Se layers contracts and Ni-Ni distances slightly expand in the K$_{0.8}$Ni$_{1.6}$Se$_2$ phase.

In order to study the effect of K and Ni vacancies on the local atomic structure, we have simulated the neutron pair-distribution functions, $G_n(r)$, for the vacancy-free and vacancy-containing systems using unit cell dimensions, atomic coordinates, and temperature factors U_{ij} given in Table I. Resulting total $G_n(r)$ from both defected and defect-free systems are presented in Fig. 2 along with the atomic pair

TABLE I. Structural parameters and mean-squared atomic displacements (U_{ij} in $10^{-2} \times \text{Å}^2$) calculated in harmonic approximation at 20 K for KNi_2Se_2 [13], $K_{0.8}Ni_2Se_2$, and $K_{0.8}Ni_{1.6}Se_2$ phases.

KNi_2Se_2		$a = 3.9714$ Å			$c = 13.1168$ Å		
Atom	Site	x	y	z	U_{11}	U_{22}	U_{33}
K	2a	0.0	0.0	0.0	0.426	0.426	0.515
Ni	4d	0.0	0.5	0.25	0.317	0.317	0.446
Se	4e	0.0	0.0	0.3507	0.228	0.228	0.383
$K_{0.8}Ni_2Se_2$		$a = 8.7773$ Å			$c = 13.3446$ Å		
Atom	Site	x	y	z	U_{11}	U_{22}	U_{33}
K	8h	0.3059	0.8860	0.0	0.438	0.480	0.484
Ni_1	4d	0.0	0.5	0.25	0.309	0.209	0.401
Ni_2	16i	0.3008	0.4000	0.2512	0.292	0.296	0.391
Se_1	4e	0.0	0.0	0.1462	0.239	0.239	0.288
Se_2	16i	0.0993	0.2994	0.3496	0.235	0.252	0.316
$K_{0.8}Ni_{1.6}Se_2$		$a = 8.9492$ Å			$c = 12.7602$ Å		
Atom	Site	x	y	z	U_{11}	U_{22}	U_{33}
K	8h	0.3120	0.8853	0.0	0.462	0.491	0.492
Ni	16i	0.3006	0.4039	0.2470	0.275	0.285	0.356
Se_1	4e	0.0	0.0	0.1493	0.244	0.244	0.267
Se_2	16i	0.1049	0.3021	0.3448	0.237	0.281	0.366

correlations (partials) for ideal KNi_2Se_2. The partial $G_n(r)$ spectra are especially useful while identifying contributions from particular atomic pairs at the given distance. Figure 2(a) indicates that in the stoichiometric KNi_2Se_2 of $I4/mmm$ symmetry, which hosts only one site for each atomic specie, the nearest neighbors of Ni atoms are Se atoms located at ~ 2.4 Å. The second neighbors of Ni atoms are Ni atoms residing at ~ 2.8 Å, but the second neighbors of Se atoms are K atoms at the distance of about 3.4 Å. Therefore, the two peaks between 2–3 Å correspond to the Ni-Se and Ni-Ni bond lengths, whereas the third peak is due to the K-Se bond length. In the $K_{0.8}Ni_2Se_2$ and $K_{0.8}Ni_{1.6}Se_2$ compositions, positions of the two first peaks are only slightly shifted with respect to those found for the stoichiometric system. This is mainly because below 3 Å the change in Ni-Se and Ni-Ni bond lengths due to incorporated cation vacancies is indeed very small (~ 0.01–0.02 Å). Also, there is no visible splitting of peaks originating from two nonequivalent Ni or Se atomic sites, in contrast to the findings made for $K_xFe_{2-y}Se_2$ counterpart [35]. The K-Se bond lengths at $r \sim 3.4$ Å remain somewhat modified in the K-deficient system, but more significant changes are encountered at distances in the range 3.4–4 Å for the composition with vacancies residing in both K and Ni sublattices. Here, a distribution of K-K, Ni-Ni, Se-Se, and K-Ni bond lengths give rise to a broad two-peak structure of the pair-distribution function. Again, pronounced differences in the $G_n(r)$ spectra of nonstoichiometric K-Ni-Se phases can be observed at distances greater than 6 Å.

B. Electronic properties

Apart from the changes in structural features of KNi_2Se_2 induced by superstructure of cation vacancies, one expects
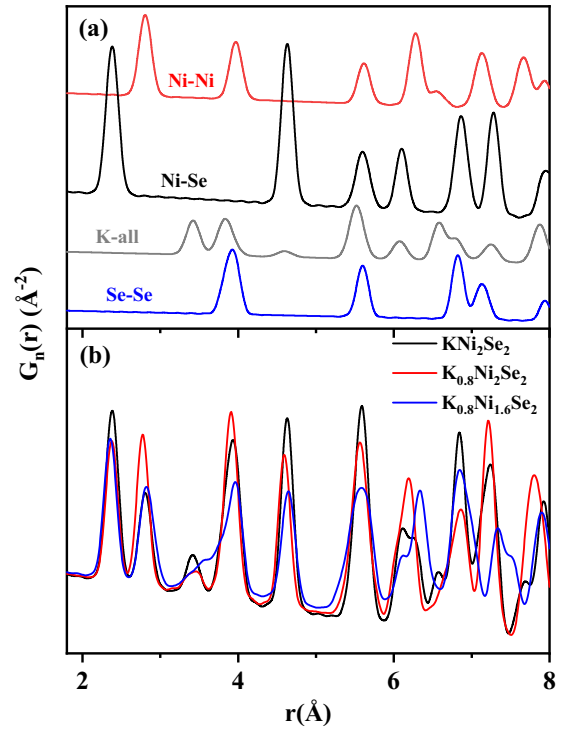
FIG. 2. (a) Partial pairwise contributions to the neutron pair-distribution function $G_n(r)$ for vacancy-free KNi_2Se_2. (b) Total $G_n(r)$ of KNi_2Se_2, $K_{0.8}Ni_2Se_2$, and $K_{0.8}Ni_{1.6}Se_2$. Simulations were performed with $Q_{max} = 35$ Å^{-1}.

some modifications of its electronic bands. To clarify such changes we first examine the band structure of stoichiometric KNi_2Se_2, which is depicted in Fig. 3(a). The valence band of KNi_2Se_2, which extends to about 6 eV below the Fermi energy (E_F), is composed of two subbands separated by a small gap. The subband ranging from E_F to -2.5 eV is dominated by the
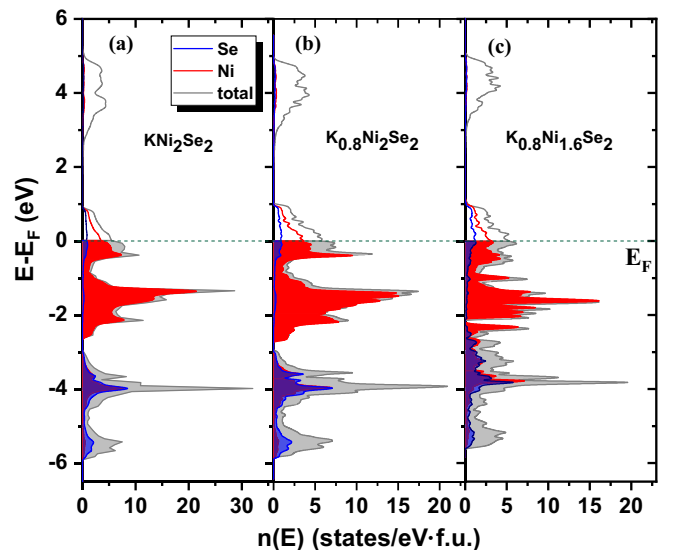
FIG. 3. Total and atomic projected electronic densities of states for (a) KNi_2Se_2, (b) $K_{0.8}Ni_2Se_2$, and (c) $K_{0.8}Ni_{1.6}Se_2$. The Fermi level E_F, indicated by dashed line, is taken as the reference energy.

Ni-3d states that are responsible for the metallic-like Ni-Ni bonds. The subband spanning between $-3\,$eV and $-6\,$eV below E_F is due to hybridized Ni-3d and Se-4p states. This hybridization gives rise to covalent bonding inside the Ni$_2$Se$_2$ layers. The mixed Ni-3d and Se-4p states constitute also the bottom of the conduction band. We note that the contribution from the K valence states to the density of electron states in KNi$_2$Se$_2$ is practically negligible. This is a common feature of the AT$_2$X$_2$ system, where the alkali atoms exist in the form of cations with valencies close to $1+$. Because of negligible contribution of the K states to the valence bands of KNi$_2$Se$_2$, defecting the K sublattice by vacancies does not change qualitatively the valence bands, as indicated by the calculated density of electron states for K$_{0.8}$Ni$_2$Se$_2$ which is presented in Fig. 3(b). More pronounced modifications of the KNi$_2$Se$_2$ valence bands occur when vacancies are introduced into the Ni sublattice. Figure 3(c) clearly shows that Ni vacancies induce additional electronic states in the vicinity of $-3\,$eV below E_F as well as cause some shift of the subband containing hybridized Ni-3d and Se-4p orbitals toward the Fermi level. Both effects lead to a closure of small gap, which separated the valence subbands in the systems with fully occupied Ni sublattice.

The K-Ni-Se systems with cation vacancies exhibit reduced spectral density at the Fermi level, $n(E_F)$, as compared to the vacancy-free KNi$_2$Se$_2$. The values of $n(E_F)$ amount to 5.99, 5.90, and 5.32 states/eV per formula unit for KNi$_2$Se$_2$, K$_{0.8}$Ni$_2$Se$_2$, and K$_{0.8}$Ni$_{1.6}$Se$_2$, respectively. On one hand, the contribution from Ni-3d states at E_F decreases with increasing vacancy concentration, but on the other hand, one observes increased contribution from the Se-4p states at E_F. which is related with the charge transfer taking place from the nickel to selenium band. This process is also reflected by the effective charges determined from the electron topological analysis [36] which gives the following effective valence charges in particular K-Ni-Se phases: K$^{0.78+}$Ni$_2^{0.28+}$Se$_2^{0.67-}$, K$_{0.8}^{0.79+}$Ni$_2^{0.28+}$Se$_2^{0.61-}$, and K$_{0.8}^{0.79+}$Ni$_{1.6}^{0.30+}$Se$_2^{0.58-}$. Furthermore, one can notice evident departure of Ni and Se valencies from their formal values (Ni^{2+}, Se^{2-}) due to the covalent bonding within the Ni$_2$Se$_2$ layers.

C. Dynamical properties

To analyze modifications of the vibrational dynamics induced by the superstructure of cation vacancies in KNi$_2$Se$_2$, we first briefly describe the main features of the phonon density of states in the vacancy-free system. The present considerations are based on our previous work [13] which addressed phonon dynamics in the defect-free KNi$_2$Se$_2$. In this work we have established that phonons in KNi$_2$Se$_2$ cover the frequency range extending up to about 216 cm^{-1}, as shown by the phonon density of states $F(\omega)$ depicted in Fig. 4. Basically, such a spectrum consists of three frequency bands, i.e., lower (LF), middle (MF), and upper (HF) ones.

The LF ($\omega \leqslant 85$ cm^{-1}) and HF ($\omega \geqslant 155$ cm^{-1}) bands are dominated by phonons arising from the shared Ni and Se atomic vibrations within the NiSe$_4$ tetrahedra which form the Ni$_2$Se$_2$ layers perpendicular to the crystallographic c axis. Within these bands the contribution from vibrations
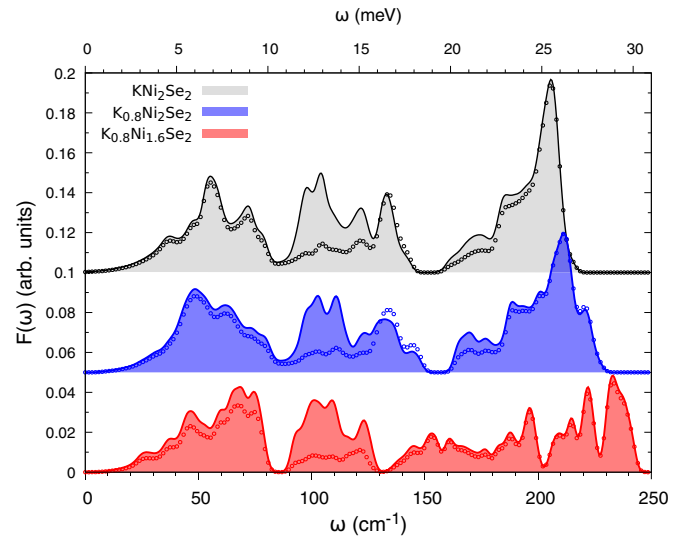
FIG. 4. *Bare* (shaded areas) and neutron-weighted (small points) densities of phonon states in KNi$_2$Se$_2$, K$_{0.8}$Ni$_2$Se$_2$, and K$_{0.8}$Ni$_{1.6}$Se$_2$ compositions.

of the K sublattice is negligible, but it becomes significant in the MF band, i.e., between 85 and 150 cm^{-1}. We also note that phonons originating from Ni and Se vibrations are not restricted to the LF and HF bands, but they contribute quite substantially to the MF band, and hence they span the entire frequency range. The LF band corresponds to the transverse and longitudinal acoustic (TA and LA) phonon modes, the MF band gathers transverse optic (TO) phonons, while the HF band, which remains separated by a small gap ($\sim$10 cm^{-1}) from the lower lying MF band is constituted by both transverse (TO) and longitudinal optic (LO) modes. No gap is, however, visible between the LF and MF bands mainly because some low-lying TO modes mix with the LA modes. It is worth noting that these characteristic features of the KNi$_2$Se$_2$ phonon spectrum are common to the ANi$_2$X$_2$ (A=K, Tl; X=Se, S) compounds and they result from their quasi-2D layered structures.

Alike spectrum of the defect-free system, the phonon spectrum of K$_{0.8}$Ni$_2$Se$_2$ also consists of three bands. Its LF and MF bands show similar spectral patterns to those observed in KNi$_2$Se$_2$. This indicates rather weak sensitivity of phonon modes with frequencies below 150 cm^{-1} to the low concentration of K vacancies ($1 - x \leqslant 0.2$). The most pronounced changes are revealed, however, in the HF phonon band. First of all, the high-frequency modes experience upward shift. One can also notice an appearance of additional phonon modes at highest frequencies. Both effects lead to effective expansion of the HF band by about 10 cm^{-1}.

Vacancies incorporated into K and Ni sublattices affect both MF and HF phonon bands, leaving the LF band almost unchanged. The MF phonon band of K$_{0.8}$Ni$_{1.6}$Se$_2$ becomes narrower by about 20 cm^{-1} than the respective bands in KNi$_2$Se$_2$ and K$_{0.8}$Ni$_2$Se$_2$, whereas its HF band significantly expands both downward and upward which is a consequence of new modes emerging in the vicinity of 150 cm^{-1} and above 220 cm^{-1}. Again, these additional modes give rise to effective broadening of the HF band. Moreover, the K$_{0.8}$Ni$_{1.6}$Se$_2$
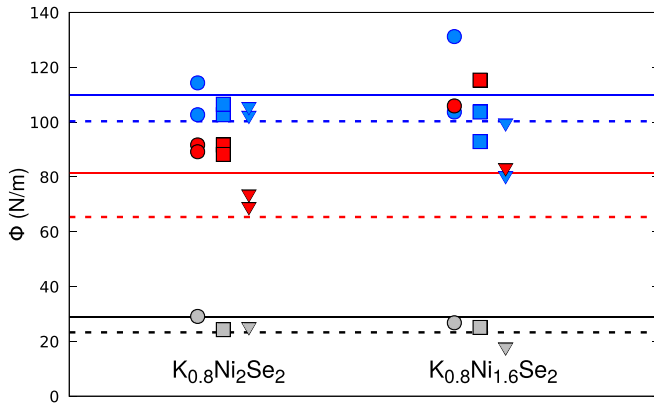
FIG. 5. The on-site force constants of K (black symbols), Ni (red symbols), and Se (blue symbols) atoms in nonstoichiometric $K_{0.8}Ni_2Se_2$ and $K_{0.8}Ni_{1.6}Se_2$ phases. The solid and dashed horizontal lines correspond, respectively, to $\Phi_{xx} = \Phi_{yy}$ and Φ_{zz} components in KNi_2Se_2 system with black, red, and blue colors denoting K, Ni, and Se atoms. The Φ_{xx}, Φ_{yy}, and Φ_{zz} components in nonstoichiometric systems are marked by circles, squares, and triangles, respectively.

spectrum exhibits diminished intensities of peaks as compared to those in vacancy-free KNi_2Se_2.

The observed effects originate mainly from structural changes caused by cation vacancies. These defects are responsible for lowering the crystal symmetry from $I4/mmm$ to $I4/m$, modifications of the atomic bonding, and atomic force constants, the latter governing dynamics of phonons. We remind that crystal lattices of K-Ni-Se phases with cation vacancies contain additional crystallographically nonequivalent Ni and Se atoms (see Table I) which leads to an emergence of additional force constants, being different from those in the defect-free phase of $I4/mmm$ symmetry. Diagonal elements of the on-site force constant matrix (Φ_{xx}, Φ_{yy}, Φ_{zz}) for each symmetry nonequivalent atom in KNi_2Se_2, $K_{0.8}Ni_2Se_2$, and $K_{0.8}Ni_{1.6}Se_2$ structures are shown in Fig. 5. They are related to the restoring force generated after the displacement of an atom in a given direction.

In both stoichiometric and nonstoichiometric K-Ni-Se phases, the force constants along the c axis (Φ_{zz}) are smaller than those perpendicular to this axis (Φ_{xx} and Φ_{yy}) which conforms to the structural features of these systems. The vacancy-containing phases exhibit increased values of the force constants at the Ni sites and slightly decreased force constants at the K sites as compared to the vacancy-free phase. On the other hand, the Se atoms in nonstoichiometric systems have both enhanced and reduced values of the force constants in comparison to those in the stoichiometric phase. These changes are, of course, more pronounced for the phase with higher vacancy concentration, which shows greater spread of the force constants than the phase with lower concentration of vacancies. The stiffening and softening of the atomic force constants with incorporation of such defects as cation vacancies give rise to modifications of the phonon frequencies that are reflected by downward and upward shift of the spectral peaks. Interestingly, the most sensitive to cation vacancies are the high-frequency optical modes.

The phonon densities of states extracted from the scattering function measured by the INS experiments will, however, be somewhat different than the calculated *bare* densities of phonon states. The main source of these differences originates from different scattering efficiencies of particular atomic species constituting sublattices of a given system. Indeed, the Ni and Se sublattices contribute in larger extent ($\sim$70% and $\sim$25%) to the neutron-weighted phonon densities of states compared to the K sublattice ($\sim$5%). Thus, the spectra in the MF range, where vibrations of the K sublattice dominate, show the most essential deviations from the *bare* $F(\omega)$, whereas in the LF and HF regimes the spectra display little change and generally follow the *bare* phonon densities of states. Hence, the INS spectra will reflect primarily the dynamics of ions within the Ni-Se layers.

The computed densities of phonon states allowed us to determine the Debye temperatures Θ_D of particular K-Ni-Se compositions. Here we relate this quantity to a second-order moment of a phonon spectrum $\langle \mu^2 \rangle$ through the following equation [37,38]:

$$\Theta_D = \frac{\hbar}{k_B} \sqrt{\frac{5}{3} \langle \mu^2 \rangle}, \tag{1}$$

where $\hbar$ and k_B have their standard meanings. The general expression for the nth moment takes on the following form [37,38]:

$$\langle \mu^n \rangle = \frac{\int \omega^n F(\omega) d\omega}{\int F(\omega) d\omega}, \tag{2}$$

while Θ_D is derived from Debye moments given by

$$\Theta_D(n) = \frac{\hbar}{k_B} \left[\frac{1}{3}(n+3)\langle \mu^n \rangle \right]^{\frac{1}{n}} \text{ for } n > -3 \text{ and } n \neq 0. \tag{3}$$

Resulting Debye temperatures amount to 210 K for KNi_2Se_2, 209 K for $K_{0.8}Ni_2Se_2$, and 204 K for $K_{0.8}Ni_{1.6}Se_2$. They closely correspond to those extracted from the heat capacity measurements ($\Theta_D \sim 210$ K) performed on stoichiometric polycrystalline KNi_2Se_2 and off-stoichiometric $K_{0.95}Ni_{1.86}Se_2$ single crystals [10,12]. Only a slight decrease in Θ_D is observed upon vacancy incorporation, and hence we may conclude that this quantity is rather weakly dependent on crystal stoichiometry as far as the K-Ni-Se system is considered.

D. Zone-center phonon modes and the Raman spectra

A detailed discussion of the phonon modes at the Γ point of the vacancy-free KNi_2Se_2 has been given in our previous work [13]. Here we pay our attention to the most important results which are relevant for understanding the influence of cation vacancies on the resulting Raman spectra.

The number of Raman, infrared (IR)-active, and inactive phonons as well as their distribution among the irreducible representations of a crystal point group can be determined by a factor group analysis. The primitive unit cell of KNi_2Se_2 contains five atoms which leads to 15 vibrational modes and the site symmetries of the K, Ni, and Se atoms in $I4/mmm$ (D_{4h}^{17}) space group are D_{4h}, D_{2d}, and C_{4v}, respectively. The Γ-point phonon modes are classified by the factor group analysis

as follows:

$$\text{K}(D_{4h}) \qquad \Gamma = A_{2u} \oplus E_u,$$

$$\text{Ni}(D_{2d}) \qquad \Gamma = E_g \oplus A_{2u} \oplus E_u,$$

$$\text{Se}(C_{4v}) \qquad \Gamma = A_{1g} \oplus B_{1g} \oplus E_g \oplus A_{2u} \oplus E_u,$$

where A_{1g}, B_{1g}, and E_g phonons are Raman active, while A_{2u} and E_u phonons are IR active. The modes with symmetries E_g and E_u remain doubly degenerate. There are no optically inactive (silent) modes in the defect-free KNi_2Se_2. Summarizing these representations and subtracting the acoustic modes (A_{2u} and E_u) one obtains the irreducible representations of the KNi_2Se_2 optical modes,

$$\Gamma_{\text{opt}} = A_{1g}(xx + yy, zz) \oplus B_{1g}(xx - yy) \oplus 2E_g(xz, yz)$$

$$\oplus 2A_{2u}(\mathbf{E} \parallel \mathbf{z}) \oplus 2E_u(\mathbf{E} \parallel \mathbf{x}, \mathbf{E} \parallel \mathbf{y}), \qquad (4)$$

where the IR-active A_{2u} and E_u modes are related to the dipole moment oscillations parallel and perpendicular to the c axis, and hence the A_{2u} (E_u) phonon can be observed in the IR spectra when the electric vector of the incident infrared radiation $\mathbf{E}$ is perpendicular (parallel) to the tetragonal ab plane. According to (4) one expects four Raman as well as four infrared modes. Note that the vibrations of K atoms do not contribute in the Raman scattering process as they are located at inversion centers.

The ordered structure of cation vacancies lowers the symmetry of $K_{0.8}Ni_2Se_2$ and $K_{0.8}Ni_{1.6}Se_2$ crystals to $I4/m$ (C_{4h}^5), and hence the number of phonon modes in these phases becomes increased. For these orthorhombic structures the factor group analysis predicts

$$\text{K}(C_s) \qquad \Gamma = 2A_g \oplus 2B_g \oplus 2E_g$$
$$\oplus A_u \oplus B_u \oplus 4E_u,$$

$$\text{Ni}_1(S_4) \qquad \Gamma = B_g \oplus 2E_g \oplus A_u \oplus 2E_u,$$

$$\text{Se}_1(C_4) \qquad \Gamma = A_g \oplus 2E_g \oplus A_u \oplus 2E_u,$$

$$\text{Ni, Ni}_2, \text{Se}_2(C_1) \qquad \Gamma = 3A_g \oplus 3B_g \oplus 6E_g$$
$$\oplus 3A_u \oplus 3B_u \oplus 6E_u,$$

where A_g, B_g, and doubly degenerate E_g modes are Raman active, A_u and doubly degenerate E_u modes are IR active, while B_u modes are silent. We note that the K atom vibrations participate in the light scattering process. Summarizing these representations and subtracting the acoustic (A_u, E_u) and silent modes one obtains the irreducible representations of the optically active vibrational modes in $K_{0.8}Ni_2Se_2$

$$\Gamma_{\text{opt}} = 9A_g(xx, yy, zz) \oplus 9B_g(xx, yy, zz)$$
$$\oplus 9E_g(xx, yy, zz) \oplus 8A_u(\mathbf{E} \parallel \mathbf{z})$$
$$\oplus 9E_u(\mathbf{E} \parallel \mathbf{x}, \mathbf{E} \parallel \mathbf{y}) \qquad (5)$$

and $K_{0.8}Ni_{1.6}Se_2$

$$\Gamma_{\text{opt}} = 9A_g(xx, yy, zz) \oplus 8B_g(xx, yy, zz)$$
$$\oplus 8E_g(xx, yy, zz) \oplus 7A_u(\mathbf{E} \parallel \mathbf{z})$$
$$\oplus 8E_u(\mathbf{E} \parallel \mathbf{x}, \mathbf{E} \parallel \mathbf{y}). \qquad (6)$$

TABLE II. Frequencies of the Raman and IR-active modes for KNi_2Se_2, $K_{0.8}Ni_2Se_2$, and $K_{0.8}Ni_{1.6}Se_2$. The numbers in brackets denote experimental [21] Raman frequencies determined for $K_{0.95}Ni_{1.86}Se_2$. For the nonstoichiometric phases, the frequencies of A_g, B_g, and E_g modes with values corresponding to the experimental A_{1g}, B_{1g}, and E_g modes are marked by (*). Units: cm^{-1}.

	Raman active			IR active	
KNi_2Se_2	A_{1g}	B_{1g}	E_g	A_{2u}	E_u
	182 (**179**)	130 (**134**)	47 (**63**)	113	102
			201	217	207
$K_{0.8}Ni_2Se_2$	A_g	B_g	E_g	A_u	E_u
	52	43	44	48	47
	73	76	55	66	72
	94	88	63*	114	100
	113	110	102	134	108
	128	129	133	173	116
	183*	132*	175	195	192
	192	198	193	209	197
	199	200	208	228	212
	217	219	211		220
$K_{0.8}Ni_{1.6}Se_2$	A_g	B_g	E_g	A_u	E_u
	52	29	46	57	45
	61	64	62*	70	76
	69	90	66	99	100
	105	119	94	166	113
	123	127*	154	200	144
	164*	159	183	218	197
	200	216	210	230	221
	205	239	232		238
	236				

According to (5) and (6), the $K_{0.8}Ni_2Se_2$ ($K_{0.8}Ni_{1.6}Se_2$) crystal is expected to show 27 (25) Raman-active and 17 (15) IR-active phonons. The calculated frequencies of the Raman and infrared phonon modes in KNi_2Se_2, $K_{0.8}Ni_2Se_2$, and $K_{0.8}Ni_{1.6}Se_2$ along with frequencies of the Raman modes measured [21] for the nonstoichiometric $K_{0.95}Ni_{1.86}Se_2$ are collected in Table II.

From a comparison of the experimental and theoretical results we find that the calculated frequencies of A_{1g} (182 cm^{-1}) and B_{1g} (130 cm^{-1}) phonons as well as those of A_g (183 cm^{-1}) and B_g (132 cm^{-1}) symmetries in $K_{0.8}Ni_2Se_2$ closely correspond to the experimental A_{1g} (179 cm^{-1}) and B_{1g} (134 cm^{-1}) phonons measured for the $K_{0.95}Ni_{1.86}Se_2$ crystal. The calculated frequencies of the A_g (164 cm^{-1}) and B_g (127 cm^{-1}) modes in $K_{0.8}Ni_{1.6}Se_2$ remain underestimated as compared to the experimental ones, even though the stoichiometry of this phase seems closer to the sample stoichiometry used in the Raman experiments [21].

On one hand, quite significant discrepancy between the measured (63 cm^{-1}) and calculated (47 cm^{-1}) frequency of the low-lying E_g mode is observed, but on the other hand, the nonstoichiometric phases exhibit some other low-lying E_g phonons with frequencies of 63 cm^{-1} ($K_{0.8}Ni_2Se_2$) and 62 cm^{-1} ($K_{0.8}Ni_{1.6}Se_2$) which are consistent with the

experimental observations. Among the high-frequency modes of E_g symmetry which are predicted for the off-stoichiometric K-Ni-Se phases, those at 193 or 208 cm^{-1} in K$_{0.8}$Ni$_2$Se$_2$ and 210 cm^{-1} in K$_{0.8}$Ni$_{1.6}$Se$_2$ seem corresponding to the high-frequency E_g mode predicted for the strictly stoichiometric system at 201 cm^{-1}. Unfortunately, the latter phonon could not be unambiguously determined by the Raman experiments [21] due to its very low intensity. Therefore, we may conclude that experimental frequencies of the zone-center phonons for the K$_{0.95}$Ni$_{1.86}$Se$_2$ structure, which was refined under symmetry constraints of $I4/mmm$ space group, can be approximated by frequencies of the K-Ni-Se phases with cation vacancies, even though the simulated structures with ordered vacancies may not fully reflect the defect structure of a real nonstoichiometric sample, in which vacancies are likely randomly distributed.

Apart from the changes in frequencies of the Raman phonons, it is interesting to analyze the effect of vacancy superstructure on the Raman modes intensities. Generally, intensities of the Raman phonons depend on the Raman tensors which take on the following form for the A_{1g}, B_{1g}, and E_g modes in KNi$_2$Se$_2$:

$$\mathbf{R}_{A_{1g}} = \begin{pmatrix} a & 0 & 0 \\ 0 & a & 0 \\ 0 & 0 & b \end{pmatrix} \qquad \mathbf{R}_{B_{1g}} = \begin{pmatrix} c & 0 & 0 \\ 0 & -c & 0 \\ 0 & 0 & 0 \end{pmatrix}$$

$$\mathbf{R}_{E_g} = \begin{pmatrix} 0 & 0 & 0 \\ 0 & 0 & e \\ 0 & e & 0 \end{pmatrix}, \qquad \begin{pmatrix} 0 & 0 & -e \\ 0 & 0 & 0 \\ -e & 0 & 0 \end{pmatrix}.$$

According to the polarization selection rules [39], the mode of A_{1g} symmetry can be observed in the polarized backscattering Raman spectra (wave vectors of incident and scattered radiations are antiparallel) when $\mathbf{e}_i \parallel \mathbf{e}_s$, while it disappears at $\mathbf{e}_i \perp \mathbf{e}_s$ (crossed) polarization configuration. Hence, the Raman spectra measured at $x(zz)\bar{x}$ or $z(x'x')\bar{z}$ scattering geometries, where $x' = \frac{1}{\sqrt{2}}[110]$, may reveal a single peak arising from the A_{1g} phonon. At the crossed polarization configuration, such as $z(x'y')\bar{z}$, where $y' = \frac{1}{\sqrt{2}}[1\bar{1}0]$, the measured spectrum can contain a single peak associated with the B_{1g} mode. Both A_{1g} and B_{1g} should be seen in the Raman spectrum taken at $z(xx)\bar{z}$ or $y(xx)\bar{y}$ scattering geometries. Also, the unpolarized Raman spectra measured from the crystal ab plane enable us to observe the mixture of A_{1g} and B_{1g} signals. Finally, determination of the E_g mode requires measurements from the crystal ac plane and a crossed polarization configuration, such as $y(zx)\bar{y}$.

Intensities of the Raman-active phonons in KNi$_2$Se$_2$ reported in our previous theoretical studies [13] correctly reproduced the experimental [21] intensity ratio between A_{1g} and B_{1g} phonons at the $z(xx)\bar{z}$ scattering geometry. Furthermore, they yielded almost negligible intensity for the E_g phonon at high-frequency, which supported experimental observation.

Due to a lower symmetry of the vacancy-containing phases, their Raman spectra are expected to show a rich spectral pattern. To calculate intensities of particular Raman modes in K$_x$Ni$_{2-y}$Se$_2$ systems with $I4/m$ symmetry, the
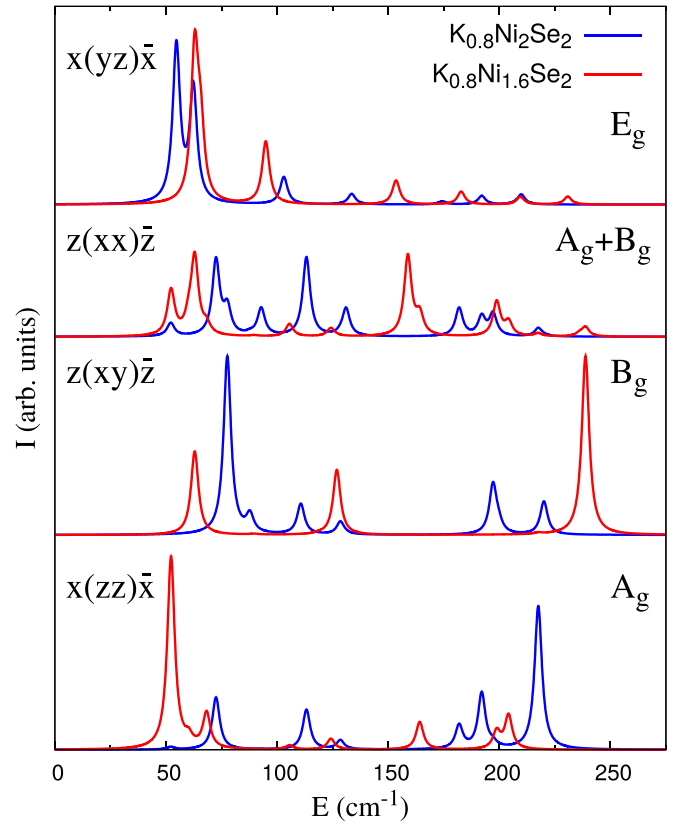
FIG. 6. Backscattering Raman spectra of nonstoichiometric K$_{0.8}$Ni$_2$Se$_2$ and K$_{0.8}$Ni$_{1.6}$Se$_2$ crystals calculated at different scattering configurations. Spectra are simulated at room temperature and with a laser excitation wavelength of 514.5 nm. Peaks are represented by Lorentzians with an artificial FHWM of 4 cm^{-1}.

following Raman polarizability tensors were considered:

$$\mathbf{R}_{A_g} = \begin{pmatrix} a & 0 & 0 \\ 0 & a & 0 \\ 0 & 0 & b \end{pmatrix} \qquad \mathbf{R}_{B_g} = \begin{pmatrix} c & d & 0 \\ d & -c & 0 \\ 0 & 0 & 0 \end{pmatrix}$$

$$\mathbf{R}_{E_g} = \begin{pmatrix} 0 & 0 & e \\ 0 & 0 & f \\ e & f & 0 \end{pmatrix}, \qquad \begin{pmatrix} 0 & 0 & -f \\ 0 & 0 & e \\ -f & e & 0 \end{pmatrix}.$$

For identification of A_g, B_g, E_g or a sum of A_g and B_g phonons from the Raman spectra of the K$_x$Ni$_{2-y}$Se$_2$ phases the same scattering geometries as those used to detect, respectively, A_{1g}, B_{1g}, E_g or a sum of A_{1g} and B_{1g} modes in strictly stoichiometric system are applicable. This is mainly because of the close correlation between $I4/mmm$ and $I4/m$ space groups. In Fig. 6, the Raman spectra of K$_x$Ni$_{2-y}$Se$_2$ under parallel and crossed polarization configurations are shown.

At $x(zz)\bar{x}$ scattering geometry the A_g phonons at 73, 113, 192, and 217 cm^{-1} yield the lines strong enough to be detected in the Raman spectrum of K$_{0.8}$Ni$_2$Se$_2$, while the most intense A_g peaks in the Raman spectrum of K$_{0.8}$Ni$_{1.6}$Se$_2$ appear at 52, 69, 169, and 205 cm^{-1}. At the crossed polarization configuration $z(xy)\bar{z}$, the B_g modes in K$_{0.8}$Ni$_2$Se$_2$ produce intense peaks at 76, 198, and 219 cm^{-1}, whereas the intense B_g peaks in the K$_{0.8}$Ni$_{1.6}$Se$_2$ spectrum are found at 64, 127, and
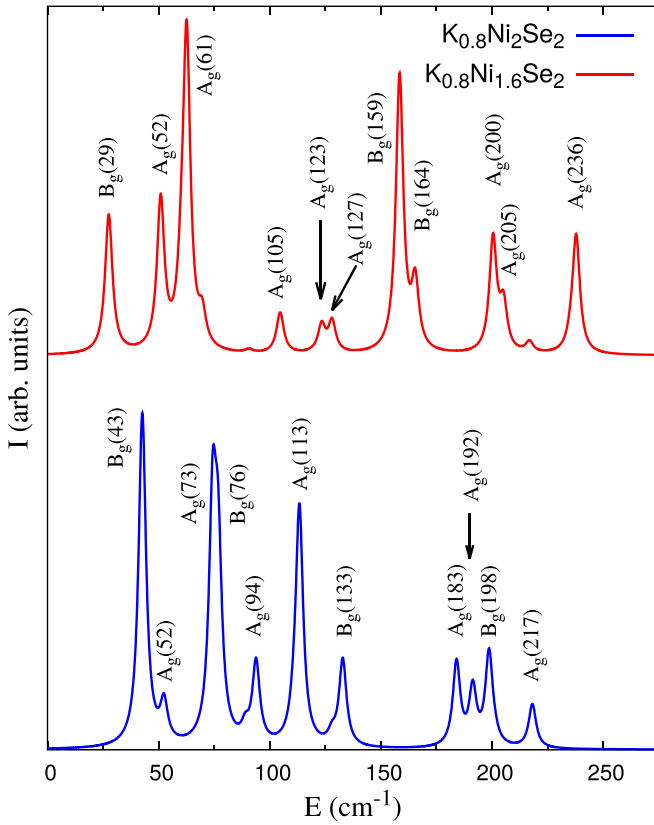
FIG. 7. Unpolarized backscattering Raman spectra of nonstoichiometric $K_{0.8}Ni_2Se_2$ and $K_{0.8}Ni_{1.6}Se_2$ crystals calculated from the crystal ab plane. Spectra are simulated at room temperature and with a laser excitation wavelength of 514.5 nm. Peaks are represented by Lorentzians with an artificial FHWM of 4 cm^{-1}. The numbers in brackets denote frequencies of modes.

FIG. 8. Unpolarized backscattering Raman spectra of nonstoichiometric $K_{0.8}Ni_2Se_2$ and $K_{0.8}Ni_{1.6}Se_2$ crystals calculated from the crystal ac plane. Spectra are simulated at room temperature and with a laser excitation wavelength of 514.5 nm. Peaks are represented by Lorentzians with an artificial FHWM of 4 cm^{-1}. Numbers in brackets denote frequencies of modes.

239 cm^{-1}. Some other A_g and B_g phonons, which are hardly detected at $x(zz)\bar{x}$ and $z(xy)\bar{z}$ geometries may be determined at $z(xx)\bar{z}$ configuration. For example, the peaks at 132 cm^{-1} in $K_{0.8}Ni_2Se_2$ and 159 cm^{-1} in $K_{0.8}Ni_{1.6}Se_2$ are assigned to B_g modes. Additionally, the peak at 181 cm^{-1} in $K_{0.8}Ni_2Se_2$ corresponds to the mode of A_g symmetry. Finally, the Raman spectra at $x(yz)\bar{x}$ scattering geometries are dominated by two peaks originating from the low-frequency E_g modes. These peaks are found at 55 and 63 cm^{-1} in the spectrum of $K_{0.8}Ni_2Se_2$ phase. At this scattering configuration, the E_g modes with detectable intensities can be observed in the spectrum of $K_{0.8}Ni_{1.6}Se_2$ at 62 and 94 cm^{-1}.

Some Raman-active modes which cannot be recorded in the polarized spectra due to their extremely low intensities are likely to be measured in experiments carried out using unpolarized light. Such spectra can be taken, for example, from the crystal ab plane. In this case the unpolarized Raman spectra of $K_{0.8}Ni_2Se_2$ or $K_{0.8}Ni_{1.6}Se_2$ monocrystals are expected to show both A_g and B_g modes, as illustrated in Fig. 7. One notes that the major contribution to the Raman spectra measured from the ac plane, Fig. 8, comes from the A_g and E_g modes. In these spectra, the B_g phonons can be present as well, but with intensities over an order of magnitude smaller than the A_g and B_g modes. Indeed, very weak features noticeable between $A_g(164)$ and $A_g(200)$ peaks or between $A_g(205)$ and

$A_g(236)$ peaks of the $K_{0.8}Ni_{1.6}Se_2$ spectrum arise from the B_g modes. Certainly, such small peaks are difficult to detect experimentally and most likely they will be hidden in the spectrum background.

A rich spectral pattern of the Raman spectra from the nonstochiometric K-Ni-Se systems may not appear when the measured compositions lack the vacancy order. The Raman spectra of K-Ni-Se phases with randomly distributed vacancies are supposed to be similar to the unpolarized Raman spectrum of the parent KNi_2Se_2 phase, albeit they would show suppressed peaks' intensities and broader FWHMs. Some shift of peaks' positions might be encountered as well. Randomly distributed defects are expected to give a similar picture to that of a disordered system which usually displays broad bands because defects lead to selection rule breakdown. In fact, the experimental Raman phonons from $K_xNi_{2-y}Se_2$ ($x = 0.95$, $y = 0.14$) [21] feature such effects. Moreover, the Raman spectra measured on $K_xCo_{2-y}Se_2$ ($x = 0.3$, $y = 0.1$), i.e., on Co-based counterpart in which no vacancy superstructure is expected, confirm such a behavior [40].

E. Heat capacity

The calculated electronic densities of states at the Fermi level could be used to determine the electronic specific heat
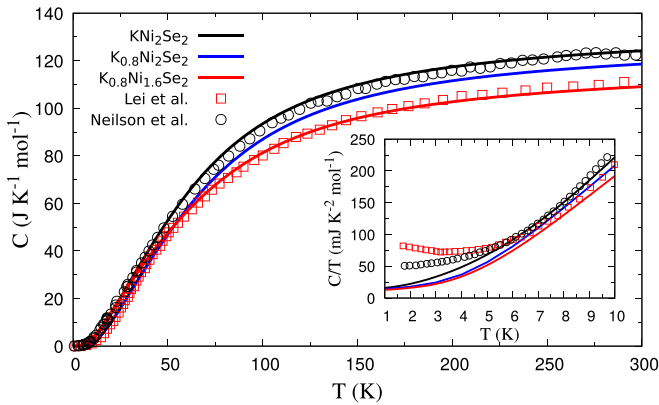
FIG. 9. Heat capacity at the constant volume of the KNi_2Se_2, $K_{0.8}Ni_2Se_2$, and $K_{0.8}Ni_{1.6}Se_2$ phases versus temperature. (Inset) Reduced heat capacity C/T of the respective K-Ni-Se phases in the low-temperature range. Experimental data denoted by open symbols are adopted from Ref. [10] (squares) and Ref. [12] (circles).

coefficient γ_0 in the approximation of free-electron gas model, where $\gamma_0 = \frac{1}{3}\pi^2 k_B n(E_F)$. The Sommerfeld coefficients of KNi_2Se_2, $K_{0.8}Ni_2Se_2$, and $K_{0.8}Ni_{1.6}Se_2$ amount to 14.14, 13.91, and 12.54 mJ/(K^2 mol), respectively. To check the effect of vacancy superstructure on the heat capacity, we took into account the electronic ($C_{el}^{(0)} = \gamma_0 T$) and lattice ($C_{ph}$) contributions to the overall heat capacity and neglected term associated with the lattice dilation because it is small below room temperature. The calculated temperature dependencies of the heat capacities for the K-Ni-Se phases along with the experimental data for the KNi_2Se_2 polycrystal [10] and $K_{0.95}Ni_{1.86}Se_2$ single crystal [12] are depicted in Fig. 9. The inset displays reduced heat capacities (C/T) of the respective systems in the low-temperature range ($T < 10$ K).

We should note that the experimental studies [10] on the polycrystalline KNi_2Se_2 revealed the λ-type behavior of the specific heat in the vicinity of 1 K, indicative of the emerging superconducting state. The critical temperature T_C was estimated to be of 0.8 K. On the other hand, no evidence of a superconducting transition down to 0.3 K has been found in resistivity measurements on $K_{0.95}Ni_{1.86}Se_2$ single crystals [12]. Nevertheless, both experimental investigations report existence of a large electronic contribution the specific heat below 20–30 K, $\gamma_{exp} = 44$–48 mJ/(K^2 mol). Significantly increased linear term is a characteristic feature of a heavy-fermion state with the effective electronic band mass enhancement $m^*/m \sim 6$–18. Therefore, at low temperatures the calculated heat capacities of KNi_2Se_2 and $K_xNi_{2-y}Se_2$ significantly differs from those provided by experiments, mainly because a renormalization of the Sommerfeld coefficient arising from the many-body effects is not captured in the present calculations. Departure of our theoretical data is especially visible below 6 K, whereas at higher temperatures it remains negligible.

Assuming that the electron-phonon interaction is the dominant many-body effect, one can estimate an enhancement factor $(1 + \lambda_{exp})$ which renormalizes electronic contribution to the specific heat according to the relation: $C_{el} = \gamma_{exp}T$, where $\gamma_{exp} = \gamma_0(1 + \lambda_{exp})$. Using the calculated γ_0 and γ_{exp}

extracted from the heat capacity measurements [10,12], an estimate for λ_{exp} of 2.1–2.5 can be obtained.

Generally, the K-Ni-Se systems with K and Ni deficiencies show lower values of the heat capacity in comparison with the defect-free system and the higher concentration of vacancies the lower heat capacity. Above 30 K the lattice term C_{ph} governs the temperature dependence of the heat capacity, and hence the phonon contribution approaches classical limit given by the equipartition law which equals 124.7 J/K mol for KNi_2Se_2, 119.7 J/K mol for $K_{0.8}Ni_2Se_2$, and 109.7 J/K mol for $K_{0.8}Ni_{1.6}Se_2$.

IV. SUMMARY AND CONCLUSIONS

The structural, electronic, and phonon properties of the $K_{0.8}Ni_2Se_2$ and $K_{0.8}Ni_{1.6}Se_2$ phases, in which cation vacancies form ordered structures, have been the subject of theoretical studies based on the density functional theory. The crystallographic and electronic structures of these nonstoichiometric phases have been shown to be distinct from those of the parent KNi_2Se_2 phase. In principle, the vacancy superstructure could be directly observed by means of the high-resolution transmission electron microscopy (HR-TEM) imaging technique.

In the daughter phases, the superstructures of cation vacancies lead to modifications of the interatomic bond lengths and force constants, and hence to changes in their vibrational dynamics which manifest via shifts and effective broadening of the phonon bands. These effects can, in principle, be detected by the inelastic neutron scattering and Raman experiments. Therefore, the present theoretical work provides simulated INS and Raman spectra of the K-Ni-Se phases with ordered cation-vacancy structures, which can serve as a guide for interpretation and refinement of respective experimental spectra, also measured on a multiphase material.

Results of our studies allow us to speculate about the influence of vacancy superstructure on the strength of electron-phonon interaction and superconductivity-related quantities in KNi_2Se_2, e.g., the superconducting critical temperature T_C. Assuming phonon-mediated superconductivity in the K-Ni-Se system which could be approximately described within the semiempirical method based on the Allen-Dynes modification of the McMillan's theory [41], usually applicable for a system with strong electron-phonon coupling ($\lambda > 1.5$) [42], we may suggest that the vacancy-containing K-Ni-Se phases would experience suppressed superconductivity. Such a conclusion can be drawn from the behavior of the density of electron states at the Fermi level as well as the Debye temperature, the latter being closely related to the average phonon frequency. Both factors undergo reduction upon incorporation of vacancies into the cation sublattice of KNi_2Se_2, but especially a decrease in the characteristic phonon frequency reflects a scattering of phonons on the defects present in the lattice. Hence, we might expect somewhat suppressed T_c in the K-Ni-Se phases with cation-vacancy superstructures as compared to the pristine material.

Despite the present research is limited to harmonic phonons, it opens a route to more complex and sophisticated studies enabling determination of the anharmonic effects [43],

which might be meaningful in the K-Ni-Se phases, not only because of their quasi-2D structure but also due to vacancy defects which are likely to induce locally strong asymmetric displacement potentials [44].

ACKNOWLEDGMENTS

[1] A. L. Ivanovskii, Phys. C **471**, 409 (2011).

[2] H.-H. Wen, Rep. Prog. Phys. **75**, 112501 (2012).

[3] D. Mou, L. Zhao, and X. Zhou, Front. Phys. **6**, 410 (2011).

[4] J. Yang, B. Chen, H. Wang, Q. Mao, M. Imai, K. Yoshimura, and M. Fang, Phys. Rev. B **88**, 064406 (2013).

[5] G. Huan and M. Greenblatt, J. Less-Common Met. **156**, 247 (1989).

[6] H.-K. Jeong, T. Valla, R. Berger, P. D. Johnson, and K. E. Smith, Europhys. Lett. **77**, 27001 (2007).

[7] R. Lizárraga, S. Ronneteg, R. Berger, A. Bergman, O. Eriksson, and L. Nordström, Phys. Rev. B **70**, 024407 (2004).

[8] U. D. Wdowik, G. Jagło, and P. Piekarz, J. Phys.: Condens. Matter **27**, 415403 (2015).

[9] G. Jagło and U. D. Wdowik, RSC Adv. **6**, 79121 (2016).

[10] J. R. Neilson, A. Llobet, A. V. Stier, L. Wu, J. Wen, J. Tao, Y. Zhu, Z. B. Tesanovic, N. P. Armitage, and T. M. McQueen, Phys. Rev. B **86**, 054512 (2012).

[11] J. R. Neilson, T. M. McQueen, A. Llobet, J. Wen, and M. R. Suchomel, Phys. Rev. B **87**, 045124 (2013).

[12] H. Lei, M. Abeykoon, K. Wang, E. S. Bozin, H. Ryu, D. Graf, J. B. Warren, and C. Petrovic, J. Phys.: Condens. Matter **26**, 015701 (2014).

[13] G. Jagło, M. Medala, and U. D. Wdowik, Phys. Lett. A **379**, 183 (2015).

[14] D. P. Shoemaker, D. Y. Chung, H. Claus, M. C. Francisco, S. Avci, A. Llobet, and M. G. Kanatzidis, Phys. Rev. B **86**, 184511 (2012).

[15] F. Ye, S. Chi, W. Bao, X. F. Wang, J. J. Ying, X. H. Chen, H. D. Wang, C. H. Dong, and M. Fang, Phys. Rev. Lett. **107**, 137003 (2011).

[16] Z. Wang, Y. J. Song, H. L. Shi, Z. W. Wang, Z. Chen, H. F. Tian, G. F. Chen, J. G. Guo, H. X. Yang, and J. Q. Li, Phys. Rev. B **83**, 140505(R) (2011).

[17] A. Ricci, N. Poccia, G. Campi, B. Joseph, G. Arrighetti, L. Barba, M. Reynolds, M. Burghammer, H. Takeya, Y. Mizuguchi, Y. Takano, M. Colapietro, N. L. Saini, and A. Bianconi, Phys. Rev. B **84**, 060511(R) (2011).

[18] M. Fang, H. Wang, C. Dong, Z. Li, C. Feng, J. Chen, and H. Yuan, Europhys. Lett. **94**, 27009 (2011).

[19] Y. J. Yan, M. Zhang, A. F. Wang, J. J. Ying, Z. Y. Li, W. Qin, X. G. Luo, J. Q. Li, J. Hu, and X. H. Chen, Nature Sci. Rep. **2**, 212 (2012).

[20] W. Li, H. Ding, P. Deng, K. Chang, C. Song, K. He, L. Wang, X. Ma, J.-P. Hu, X. Chen, and Q.-K. Xue, Nat. Phys. **8**, 126 (2012).

[21] N. Lazarević, M. Radonjić, M. Šćepanović, H. Lei, D. Tanasković, C. Petrovic, and Z. V. Popović, Phys. Rev. B **87**, 144305 (2013).

[22] J. R. Neilson and T. M. McQueen, J. Am. Chem. Soc. **134**, 7750 (2012).

[23] V. V. Bannikov and A. L. Ivanovskii, Physica C **492**, 44 (2012).

[24] G. Kresse and J. Furthmüller, Phys. Rev. B **54**, 11169 (1996); Comput. Mater. Sci. **6**, 15 (1996).

[25] J. P. Perdew, K. Burke, and M. Ernzerhof, Phys. Rev. Lett. **77**, 3865 (1996); **78**, 1396 (1997).

[26] P. E. Blöchl, Phys. Rev. B **50**, 17953 (1994); G. Kresse and D. Joubert, *ibid.* **59**, 1758 (1999).

[27] K. Parlinski, Z. Q. Li, and Y. Kawazoe, Phys. Rev. Lett. **78**, 4063 (1997); K. Parlinski, *Software PHONON ver. 6.15*, Cracow, Poland (2015).

[28] M. Cardona, ed., *Light Scattering in Solids I*, Vol. 8 (Springer-Verlag, Berlin Heidelberg, 1983).

[29] P. Umari, A. Pasquarello, and A. DalCorso, Phys. Rev. B **63**, 094305 (2001); P. Umari, X. Gonze, and A. Pasquarello, Phys. Rev. Lett. **90**, 027401 (2003).

[30] M. Gajdoš, K. Hummer, G. Kresse, J. Furthmüller, and F. Bechstedt, Phys. Rev. B **73**, 045112 (2006).

[31] P. Juhás, T. Davis, C. L. Farrow, and S. J. L. Billinge, J. Appl. Crystallogr. **46**, 560 (2013); C. L. Farrow, P. Juhás, J. W. Liu, D. Bryndin, E. S. Božin, J. Bloch, T. Proffen, and S. J. L. Billinge, J. Phys.: Condens. Matter **19**, 335219 (2007); T. Proffen and S. J. L. Billinge, J. Appl. Crystallogr. **32**, 572 (1999).

[32] S. W. Lovesey, *Theory of Neutron Scattering from Condensed Matter* (Oxford University Press, Oxford, 1987), Chap. 4.

[33] V. F. Sears, Neutron News **3**, 26 (1992).

[34] R. Mittal, M. K. Gupta, S. L. Chaplot, M. Zbiri, S. Rols, H. Schober, Y. Su, T. Brueckel, and T. Wolf, Phys. Rev. B **87**, 184502 (2013).

[35] D. Louca, K. Park, B. Li, J. Neuefeind, and J. Yan, Sci. Rep. **3**, 2047 (2013).

[36] R. Bader, *Atoms in Molecules: A quantum Theory* (Oxford University Press, New York, 1990).

[37] G. Grimvall, *Thermophysical Properties of Materials* (North Holland, Amsterdam, 1986).

[38] R. Pässler, J. Appl. Phys. **101**, 093513 (2007).

[39] R. Loudon, Adv. Phys. **50**, 813 (2001).

[40] M. Opačić, N. Lazarević, M. M. Radonjić, M. Šćepanović, H. Ryu, A. Wang, D. Tanasković, C. Petrovic, and Z. V. Popović, J. Phys.: Condens. Matter **28**, 485401 (2016).

[41] W. L. McMillan, Phys. Rev. **167**, 331 (1968); P. B. Allen and R. C. Dynes, Phys. Rev. B **12**, 905 (1975).

[42] G. Grimvall, Phys. Scr. **14**, 63 (1976).

[43] K. Parlinski, Phys. Rev. B **98**, 054305 (2018).

[44] A. Glensk, B. Grabowski, T. Hickel, and J. Neugebauer, Phys. Rev. X **4**, 011018 (2014).